J Arid Land (2023) 15(11): 1269–1289
https://doi.org/10.1007/s40333-023-0110-8

Science Press Springer-Verlag

Combining RUSLE model and the vegetation health index to unravel the relationship between soil erosion and droughts in southeastern Tunisia

Olfa TERWAYET BAYOULI[1,2], ZHANG Wanchang[1,2*], Houssem TERWAYET BAYOULI[3]

[1] Key Laboratory of Digital Earth Science, Aerospace Information Research Institute, Chinese Academy of Sciences, Beijing 100094, China;
[2] University of Chinese Academy of Sciences, Beijing 100049, China;
[3] National Agronomic Institute of Tunisia (INAT), Tunis 1082, Tunisia

Abstract: Droughts and soil erosion are among the most prominent climatic driven hazards in drylands, leading to detrimental environmental impacts, such as degraded lands, deteriorated ecosystem services and biodiversity, and increased greenhouse gas emissions. In response to the current lack of studies combining drought conditions and soil erosion processes, in this study, we developed a comprehensive Geographic Information System (GIS)-based approach to assess soil erosion and droughts, thereby revealing the relationship between soil erosion and droughts under an arid climate. The vegetation condition index (VCI) and temperature condition index (TCI) derived respectively from the enhanced vegetation index (EVI) MOD13A2 and land surface temperature (LST) MOD11A2 products were combined to generate the vegetation health index (VHI). The VHI has been conceived as an efficient tool to monitor droughts in the Negueb watershed, southeastern Tunisia. The revised universal soil loss equation (RUSLE) model was applied to quantitatively estimate soil erosion. The relationship between soil erosion and droughts was investigated through Pearson correlation. Results exhibited that the Negueb watershed experienced recurrent mild to extreme drought during 2000–2016. The average soil erosion rate was determined to be 1.8 t/(hm^2·a). The mountainous western part of the watershed was the most vulnerable not only to soil erosion but also to droughts. The slope length and steepness factor was shown to be the most significant controlling parameter driving soil erosion. The relationship between droughts and soil erosion had a positive correlation (r=0.3); however, the correlation was highly varied spatially across the watershed. Drought was linked to soil erosion in the Negueb watershed. The current study provides insight for natural disaster risk assessment, land managers, and stake-holders to apply appropriate management measures to promote sustainable development goals in fragile environments.

Keywords: droughts; soil erosion; vegetation health index (VHI); revised universal soil loss equation (RUSLE) model; southeastern Tunisia

Citation: Olfa TERWAYET BAYOULI, ZHANG Wanchang, Houssem TERWAYET BAYOULI. 2023. Combining RUSLE model and the vegetation health index to unravel the relationship between soil erosion and droughts in southeastern Tunisia. Journal of Arid Land, 15(11): 1269–1289. https://doi.org/10.1007/s40333-023-0110-8

1 Introduction

Droughts and soil erosion triggered by climate change were identified as the greatest challenge to sustainable development in arid and semi-arid regions (Rahmati et al., 2017; Lucatello and Huber-Sannwald, 2020; Abdelhak, 2022; Wu et al., 2022). Drought is the most common natural

*Corresponding author: Wanchang Zhang (E-mail: zhangwc@radi.ac.cn)
Received 2022-12-05; revised 2023-08-02; accepted 2023-08-24

hazard, and poses a worldwide threat to agriculture and water resources (Lloyd-Hughes, 2013). Due to the complex and multidimensional nature of droughts, numerous indices have been developed (Zargar et al., 2011; Bayissa et al., 2021). Single or combined, these indices can assign droughts identification with respect to duration, severity, intensity, and location (Heim, 2002; Keyantash and Dracup, 2002). Although the standardized precipitation index (SPI), a precipitation-based index, is the most commonly used, remote sensing-based indices are increasingly important tools for droughts monitoring as they can surpass the limitations of other indices which often require multiple and serially complete data (Hazaymeh and Hassan, 2017; Marumbwa et al., 2020).

In arid regions, issues related to natural resource degradation involve not only droughts but also soil erosion, which is recognized as another major environmental problem (Du et al., 2016). Soil erosion is a result of complex processes stemming from natural and anthropogenic activities, and is expected to expand steadily (Eekhout and de Vente, 2022). Soil erosion constitutes a serious threat to agriculture, water security, and ecosystem services that can also exacerbate drought effects (Patil, 2018; Qiu et al., 2021). Over the last decade, several approaches have been developed for estimating soil erosion. These approaches include empirical and physical models. The revised universal soil loss equation (RUSLE) model developed by Renard et al. (1997) has been one of the most widely applied models, due to its simplicity and robustness. It confers erosion rates estimation in a given watershed considering the climatic and environmental characteristics. The RUSLE model includes five input factors: erosivity, soil erodibility, slope length and steepness, land cover, and erosion control practices (Renard et al., 2017). These factors vary spatiotemporally and are dependent on other variables (Prasannakumar et al., 2012).

Compared to other Mediterranean countries, droughts and soil erosion arise crucial environmental concerns in Tunisia, particularly in its southern arid regions. Climate change and global warming have exacerbated these concerns resulting in a reduction of vegetation cover, increased soil erosion, and a decline in biological diversity (Sghaier et al., 2012). Tunisia, with about 1.0×10^7 hm^2 under agricultural use, faces water erosion threats to nearly 3.0×10^6 hm^2 of agricultural soils (Kefi et al., 2012). Despite its aridity, water erosion is the most widespread degradation feature in southeastern Tunisia. This results from heavy and torrential rainfall that generates intense runoff, shallow soils, low water storage capacity, and precarious vegetation cover (Taamallah, 2003; Gamoun, 2016). The Negueb watershed is one of the main watersheds of Medenine Governorate in southeastern Tunisia and is susceptible to soil erosion as evidenced by highly pronounced physical features. Simultaneously, the watershed is experiencing recurrent droughts of increasing intensity, with broader deleterious impacts on agriculture and water resources (Verner et al., 2018). There are several links between soil erosion and droughts. Soil erosion is one of major land degradation drivers, resulting from prior dry conditions, which negatively affected ecosystem services (Peri et al., 2021). Droughts exacerbate soil erosion by intensifying sand and runoff activities (Trnka et al., 2016; Middleton and Kang, 2017). Moreover, droughts impede vegetation growth, especially in arid regions, leading to soil organic carbon depletion. This reduction in carbon matter is a negative feedback, combined with the soil structure disruption, which further exacerbates soil erosion (da Silva et al., 2013). Soil erosion results in topsoil loss, which is generally richest in organic matter and nutrients. For example, it has been shown that the distribution of soil organic carbon loss was correlated with soil erosion risk classes in the central Black Sea region, Turkey (Imamoglu and Dengiz, 2017). The drought-induced land use changes, such as the conversion of wetlands or croplands to barren lands, disrupt the water cycle and hydrological functions, which could enhance soil erodibility, especially during long-lasting droughts. Additionally, soil erosion may also increase vulnerability to droughts by amplifying drought effects due to the altered hydrology that leads to poorer soil quality (Reichhuber et al., 2019).

Despite the importance of the issue, the literature investigating the connection between soil erosion and droughts remains limited. Globally, few studies directly addressed the interrelationship between droughts and soil erosion. For instance, Santra and Mitra (2020) found

that the areas with high drought frequency experienced almost double the rate of soil loss as the areas with low drought frequency in west Bengal, India. Other studies carried out in Southwest China and western India reported a positive relationship between soil erosion and droughts (Yu et al., 2021; Masroor et al., 2022). Despite the troubling natural resource degradation induced chiefly by soil erosion and droughts in the Negueb watershed, studies devoted to their assessment remain very limited and the relationship between droughts and soil erosion remains unresolved. It is therefore necessary to develop methods integrating the principal factors that trigger, simultaneously, droughts and soil erosion. In this study, we propose that extended periods of droughts will cause higher soil erosion. Droughts will also reduce vegetation cover, creating a negative feedback loop that further elevates the risk of soil erosion. Thus, this study aims to (1) assess drought conditions in the Negueb watershed from 2000 to 2016; (2) estimate soil erosion rates in the watershed; and (3) reveal the relationship between soil erosion and droughts. The results of this study will support natural disaster risk assessment for better management of soil erosion and drought effects in arid fragile environments.

2 Materials and methods

2.1 Study area

The Negueb watershed is within the large Oum Zassar basin, which is among the most important basins of the Tunisian Jeffara due to its drainage dense network (Fig. 1). The watershed is located in southeastern Tunisia (33°25′–33°60′N, 10°00′–10°22′E), and generally drains to the east from high-elevation steep-slope upstream (<690 m) into foothills with medium (<10%) to low (<5%) slopes into the Mediterranean Sea. The Negueb watershed crosscuts two climate zones: Mediterranean and arid climate (Floret and Pontanier, 1982). The study area receives a mean annual precipitation of 200 mm, has an annual mean temperature of 22°C, with spatiotemporally irregular and torrential rainfall (Schiettecatte et al., 2005; Genin et al., 2006). The hierarchical hydrographic network is composed of series of wadis flowing from the Matmatas Mountains. The poorly developed soils have formed on limestone substratum in the upstream and grade to gypseous to gypseous-limestone at the downstream, forming mainly Leptosols, Regosols, and Arenosols (FAO, 2015). The vegetation is sparse and stunted characterized by Chamaephytes steppes (Gamoun, 2016). Therefore, the studied watershed is vulnerable to highly pronounced soil erosion and droughts. Within the watershed, the main land use/land cover (LULC) categories are croplands, rangelands, and bare soils. In response to ongoing degradation problems, sustainable land management practices have been instituted to combat land degradation and drought effects (König et al., 2012).

2.2 Data collection

This study combined two important land degradation features impacting southeastern Tunisia, droughts and soil erosion. To access droughts, we collected moderate resolution imaging spectroradiometer (MODIS) land surface temperature (LST) MOD11A2 and enhanced vegetation index (EVI) MOD13A2 images with a 1-km spatial resolution from 2000 to 2016 (https://www.earthdata.nasa.gov/eosdis/daacs/laads). The EVI and LST data were used to derive the vegetation condition index (VCI) and temperature condition index (TCI), respectively, and the VCI and TCI were combined to generate the vegetation health index (VHI). To access soil erosion, we used the RUSLE model, which incorporates five factors (i.e., erosivity, soil erodibility, slope length and steepness, land cover, and erosion control practices). To compute the erosivity factor, we collected a 48-year historical monthly precipitation record (1968–2016) from local hydrological databases. For slope estimation, shuttle radar topography mission (SRTM) image with a 30-m resolution was used for elevation information. The soil map and the hydrographic network were obtained from the regional agricultural map of Medenine Governorate. Satellite images with a 30-m resolution from Landsat 8 Operational Land Imager (OLI) and Thermal Infrared Sensor (TIRS) were used to generate a LULC map. These datasets

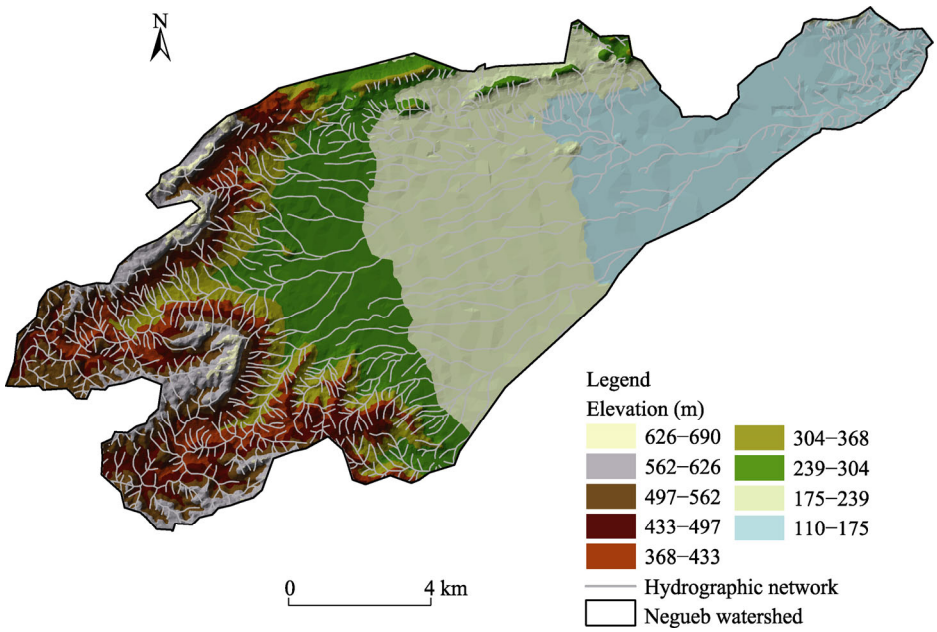

Fig. 1 Overview of the study area

were incorporated into a geographic information system (GIS) environment to compute the RUSLE model for estimating soil loss rates in the Negueb watershed.

2.3 Drought characteristics assessment

The fundamental drought characteristics (intensity, duration, frequency, and location) were determined from 2000 to 2016 (Table 1) (Zhang et al., 2015).

Table 1 Drought characteristics used in this study

Drought parameter	Equation	Symbol and unit
Area	$D_a = \frac{\sum_{i=1}^{n} da}{n} \times 100\%$	D_a is the drought area (%); da is the number of pixels with the vegetation health index (VHI) greater than 40; and n is the total number of pixels.
Duration	$D = \frac{\sum_{i=1}^{n} di}{m}$	D is the drought duration (month); di is the duration of i^{th} drought event; and m is the total number of drought events.
Frequency	$F = \frac{n_m}{N_m} \times 100\%$	F is the drought frequency (%); n_m is the number of drought months (month); and N_m is the total number of months (month).
Intensity	$I = \left\lvert \frac{1}{N_m} \sum_{i=1}^{z} \mathrm{VHI}_i \right\rvert$	I is the drought intensity; N_m is the total number of months (month); z is the number of drought occurrences in months with the VHI greater than 40; and VHI_i is the VHI value below the threshold (40).

2.3.1 Vegetation condition index (VCI)

The VCI (%) compares the actual vegetation state to an historical range of values observed within the same period (Liu and Kogan, 1996). The VCI indicates the vegetation growth conditions over time. High VCI values reflect a healthy vegetation state, whereas low VCI values designate poor vegetation conditions. The VCI provides indirect insight about drought conditions. In this study, the EVI was employed to derive the VCI. The MOD13A2 EVI data were selected, taking into account the background and atmospheric effects, for their capacity for highlighting the spectral response related to green vegetation canopy. The VCI was calculated as follows:

$$\mathrm{VCI}_i = \frac{\mathrm{EVI}_i - \mathrm{EVI}_{\min}}{\mathrm{EVI}_{\max} - \mathrm{EVI}_{\min}} \times 100\% , \quad (1)$$

where VCI_i is the VCI of a certain month (%); EVI_i is the EVI of a certain month; and $\mathrm{EVI}_{\min}$ and

EVI_{max} are the minimum and maximum EVI values in the corresponding month in the studied period, respectively.

2.3.2 Temperature condition index (TCI)

The LST is considered a key indicator of drought. High and low LST values during the growing season reflect drought and drought-free conditions, respectively (Singh et al., 2003). However, the LST alone is not entirely capable of assessing droughts since it is sensitive to environmental and atmospheric conditions (Shen et al., 2019). The TCI captures the state of vegetation under high temperature and water stress on the soil surface (Kogan, 1995). The relative TCI measurement is based on brightness thermal temperature from the LST measurements, and the low TCI refers to more severe droughts (Singh et al., 2003). We computed the TCI retrieved from MOD11A2 LST according to the following formula:

$$TCI_i = \frac{LST_i - LST_{min}}{LST_{max} - LST_{min}} \times 100\%, \quad (2)$$

where TCI_i is the TCI of a certain month (%); LST_i is the LST of a certain month (K); and TCI_{max} and TCI_{min} are the maximum and minimum TCI values for the corresponding month in the study period, respectively (Kogan, 1995).

2.3.3 Vegetation health index (VHI)

The VHI identifies general vegetation health. It involves the VCI and TCI, which considers both moisture availability and thermal conditions in vegetation. By integrating the thermal component along with the vegetation component, the VHI provides a more comprehensive assessment of drought condition (Seiler et al., 1998). This combination has yielded acceptable results for drought monitoring across different soil climate regimes, particularly in arid regions (Karnieli et al., 2006; Rhee et al., 2010; Parviz, 2016; Ghoneim et al., 2017). The VHI calculation is as follows:

$$VHI = \alpha(TCI) + \alpha(VCI), \quad (3)$$

where the VHI is determined by a weighted contribution (α) of the VCI and TCI (Bento et al., 2020). The weighting cannot be accurately determined as it varies according to the location and time. Thus, it was assumed to be equal contributions of 0.5 for both indices (Kogan et al., 2016; Gidey et al., 2018; Pei et al., 2018; Bento et al., 2020). In this study, the widely used VHI classification scheme of Kogan (1995) was adopted (Table 2). The VHI values range from 0 (extreme drought) to >40 (no drought). The VHI values were calculated for March during the assessment period (2000–2016). We calculated the coefficient of variation (CV) and the mean of VHI to assess the consistency of drought spatial distribution.

Table 2 Classification of the vegetation health index (VHI)

VHI value	Drought condition
<10	Extreme drought
10–20	Severe drought
20–30	Moderate drought
30–40	Mild drought
>40	No drought

Note: Classification of the VHI comes from Kogan (1995).

2.4 Soil erosion estimation

The RUSLE model developed by Renard et al. (1997) is the most widely used model for annual average soil loss prediction (Borrelli et al., 2017). It was selected in this study due to its simplicity and agreement in terms of data requirements and application, and because it is applicable across wide and diverse scales, particularly in the arid regions of the Mediterranean basin including Tunisia (Omuto and Vargas, 2009; Kefi et al., 2012; Ben Rhouma et al., 2018;

Amellah and el Morabiti, 2021; Jemai et al., 2021; Bensekhria and Bouhata, 2022). The RUSLE model is a function of five input factors in raster data format, and it can be expressed as follows:

$$A = R\ \text{factor} \times K\ \text{factor} \times LS\ \text{factor} \times C\ \text{factor} \times P\ \text{factor}, \quad (4)$$

where A is the average annual soil loss per unit area (t/(hm^2·a)); R factor is rainfall erosivity factor (MJ·mm/(hm^2·h·a)); K factor is soil erosivity factor (t·hm^2·h/(hm^2·MJ·mm)); LS factor is slope length and steepness factor; C factor is cover management factor; and P factor is conservation support practice factor.

To improve the applicability of RUSLE model in the study area, we selected the input parameters from reliable local databases and field observations. A geodatabase including codified and structured RUSLE factors data was created. The cell size of all generated data was maintained at 20 m to create a uniform spatial GIS analysis environment. The adopted overall methodology is represented in Figure 2.

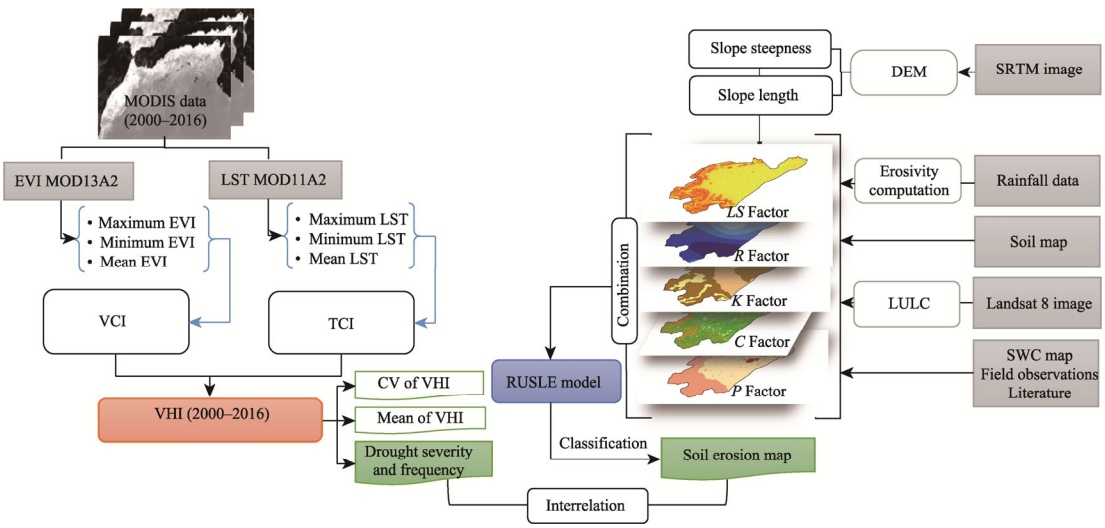

Fig. 2 Flowchart of the methodology used in this study. VHI, vegetation health index; TCI, temperature condition index; VCI, vegetation condition index; EVI, enhanced vegetation index; LST, land surface temperature; CV, coefficient of variation; SWC, soil and water conservation; A, the average annual soil loss per unit area; R factor, rainfall erosivity factor; K factor, soil erosivity factor; LS factor, slope length and steepness factor; C factor, cover management factor; P factor, conservation support practice factor; MODIS, moderate resolution imaging spectroradiometer; RUSLE, revised universal soil loss equation; DEM, digital elevation model; SRTM, shuttle radar topography mission; LULC, land use/land cover.

2.4.1 Rainfall erosivity factor (R factor)

Rainfall erosivity is defined as the potential rainfall ability to cause erosion. The rainfall erosivity factor (R factor; MJ·mm/(hm^2·h·a)) quantifies the impact of rainfall and induced runoff on the soil (Brychta et al., 2022). For a given period, we can estimate the R factor according to the following formula (Wischmeier and Smith, 1978):

$$R\ \text{factor} = Ec \times I30, \quad (5)$$

where Ec is the rainfall kinetic energy (MJ/hm^2) and $I30$ is the maximum rainfall intensity in 30 min (mm/h).

Although the lack of rainfall data in the study area may lead to inaccurate calculations of R factor, a simplified empirical formula that correlates the R factor with more readily available parameters such as average annual rainfall or Fournier index was used to determine the values of R factor (Table 3).

2.4.2 Soil erodibility factor (K factor)

The soil erodibility factor (K factor; t·hm^2·h/(hm^2·MJ·mm)) refers to the cohesion and resistance of soils to erosion. It depends mainly on the soil texture, structure, organic matter (OM) content,

Table 3 Calculation of the rainfall erosivity factor (*R* factor)

Model	Reference	Model	Reference
$R = 0.264 \times \mathrm{MFI}^{1.5}$	Arnoldus (1977)	$R = 36.46 + 1.84 \times \mathrm{MFI} - 0.158 \times \mathrm{P}$	Ferro et al. (1991)
$R = 587.9 - 1.219 \times \mathrm{P} + 0.004105 \times \mathrm{P}^2$ for P>850 mm/a	Renard and Freimund (1994)	$R = b_0 + b_1 \times \mathrm{P} + b_2 \times \mathrm{P}^2$ *f*or P>850 mm/a, where b_0=0.0483 MJ/(hm²·h)); b_1=1.610; and b_2=0.004105.	Yang et al. (2003)
$R = 0.87 - 0.037 \times \mathrm{P} + 0.016 \times \mathrm{P}^2$	Pepin and Hammouda (2012)	$R = b_0 \times \mathrm{P}^2 \times \sqrt{P} \times (\alpha \times b_1 \times \mathrm{L})$, where α=2; b_0=0.117; b_1= –0.015.	Diodato and Bellocchi (2010)
$R = 168.42 + 3.27 \times \mathrm{MFI}$	Roose (1977)	$R = 1.042 \times \mathrm{MFI}^{1.59}$	Belaid and Habaieb (2015)
$R = 15.485 + 0.602 \times \mathrm{MFI}$	DVWK (1990)		

Note: *R*, *R* factor; MFI, modified Fournier index; P, precipitation; L, longitude. These formulas are adapted to Mediterranean climatic conditions; and we applied these formulas to 12 stations in the studied watershed based on rainfall data availability in a given period.

and permeability (Renard et al., 1997). In this study, we obtained a soil map based on the French soil classification system from the agricultural map of Medenine Governorate. Although the soils had low OM content, they exhibited notable differentiation and diversity. However, their texture and structure were susceptible to disturbance, particularly from the factors like water and wind erosion. Four main classes were recognized (Table 4). Firstly, raw mineral soils (Lithosols or Regosols), which are shallow soils, sandy to sandy-loamy, with low OM content and very high stone load on the surface. They are mainly composed of dolomites, limestone outcroppings, and stony regs (Mtimet, 2001). Secondly, slightly evolved alluvial soils. These are deep (>1.50 m) with a silty-loam to sandy texture, and the OM content does not exceed 0.5% (Mtimet, 2001). Thirdly, isohumic soils, which show morpho-analytical characteristics of fine sands, coarse silts, and a poor structural stability. This soil type initiates rill and gully erosion. They are not very deep and can be covered by a shallow wind deposit and have low OM content, high surface stone-load with very deep supply soils in the supply zones (Genin et al., 2006). Fourthly, composed soils of sandy to sandy-loamy with river deposits made up of loess, terraces, and sometimes dunes have low OM content, are not very deep, and occupy a relatively small area at the plain (Taamallah, 2003).

Table 4 Soil erodibility factor (*K* factor) of different soil types in the Negueb watershed

Soil type	*K* factor (t·hm²·h/(hm²·MJ·mm))	Soil type	*K* factor (t·hm²·h/(hm²·MJ·mm))
Raw mineral soils (Lithosols or Regosols)	0.036	Isohumic soils	0.054
Slightly evolved alluvial soils	0.080	Composed soils	0.050

2.4.3 Slope length and steepness factor (*LS* factor)

The slope length and steepness factor (*LS* factor) considers both the slope length and steepness, being responsible for generating and transporting sediments, respectively, in a watershed (Liu et al., 2000). Soil loss per unit area depends on these factors and increases with the slope length and steepness (Lu et al., 2020). The *LS* factor is defined as the ratio of soil damage on a certain slope length and steepness relative to soil loss from a slope with a length of 22.1 m and a steepness of 9% (Renard et al., 1997). The equation is as follows:

$$LS \text{ factor} = \left(\frac{\lambda}{22.13} \right)^m \times S , \tag{6}$$

where λ is slope length (m); S is slope steepness (%); and m is slope-length factor. The computation of *LS* factor is complicated as it incorporates several parameters, particularly terrain slopes. Here, this factor was determined using the digital elevation model (DEM) from SRTM, which was processed using SAGA GIS software. SAGA GIS uses the DEM to calculate the slope degree, orientation, and cumulative length to compute the *LS* factor.

2.4.4 Cover management factor (*C* factor)

Vegetation cover is another factor controlling soil erosion as densely vegetated soils have greater erosion resistance than sparsely vegetated soils (Tamene and Le, 2015). Cover management is defined as the ratio of soil loss from land with a certain vegetation type to the equivalent soil loss from tilled and bare soils (Wischmeier and Smith, 1978). The cover management factor (*C* factor) map was developed from a LULC map of the Negueb watershed. This LULC map was produced from Landsat 8 image of 2014 (normal hydrological year) with a 30-m resolution, on the basis of supervised classification and field observations. The values of *C* factor assigned to the LULC categories of the Negueb watershed were determined from the study conducted by Cormary and Masson (1964), who defined this factor for the different LULC types in Tunisia (Table 5).

Table 5 Classification of land use/land cover (LULC) types and cover management factor (*C* factor)

LULC type	*C* facor	LULC type	*C* facor
Croplands behind Jessours	0.18	Bedrocks	0.90
Croplands behind Tabias	0.18	Bare soils	1.00
Rangelands	0.55		

Note: Jessours and Tabias are traditional soil and water conservation technique used for growing crops and fruit trees.

2.4.5 Conservation support practice factor (*P* factor)

The conservation support practice factor (*P* factor) introduces the anti-erosive practices that mitigate water erosion induced by surface runoff (Renard et al., 1997), with the values of *P* factor ranging between 0.00 and 1.00, where 0.00 represents a strong resistance to soil erosion and 1.00 reflects the absence of anti-erosion practices (Table 6) (Fang et al., 2019). The *P* factor map was produced from the LULC map and terrain observations. The anti-erosion practices in the watershed were essentially bench terraces and retention bench terraces. The values of *P* factor retained for the Negueb watershed were based on studies carried out by Food and Agricultural Organization in Tunisia (FAO, 1977).

Table 6 Conservation support practice factor (*P* factor) for different anti-erosion practices with slope ranges

Anti-erosion practice	*P* factor	Anti-erosion practice	*P* factor
Bench terraces with or without plantations (5%–10%)	0.10	Retention bench terraces (0%–5%)	0.10
Bench terraces with or without plantations (15%–20%)	0.16	Retention bench terraces (5%–15%)	0.12
Bench terraces with or without plantations (20%–30%)	0.18	Retention bench terraces (15%–25%)	0.16

Note: Figures in brackets represent slope ranges.

2.4.6 Validation of RUSLE model results

Validating RUSLE model results in arid environments can be challenging due to the unique characteristics of these regions, such as low vegetation cover, sparse rainfall, and high evapotranspiration rates, and the scarcity of available data for comparing the model estimates with actual soil losses (Lazzari et al., 2015). In this study, along with intensive field observations, we took advantage of the availability of high-resolution remote sensing imagery to validate the erosion risk map. A spatial scale validation was first conducted through photointerpretation in the software packages (TerraIncognita and Google Earth). Ground truthing of eroded areas was verified in the field by precise location using global positioning system (GPS) to compare representative sample points from the erosion risk map with field observations classified by erosion categories. Local experts classified the ground points into three categories based on the effects and signs of soil erosion. The first category, labeled as "low", indicates slight erosion resulting from sheet erosion. The second category, labeled as "moderate", had impacts of both sheet and rill erosion leading to topsoil loss. The third category, labeled as "severe", was identified by the removal of most of the topsoil due to sheet and rill erosion. RUSLE model outputs were further endorsed by comparison to other local studies having similar characteristics to our study area (MEHAT, 2012; Jemai et al., 2021).

3 Results

3.1 Drought characterization

In this study, drought conditions have been examined by means of the VHI from 2000 to 2016 (Fig. 3). The growing season in Tunisia is from November to April; however, rainfall in March is a critical factor for soil moisture according to the local agricultural experts. Thus, a series of the VCI and TCI maps for March were created using the EVI and LST data, respectively, during 2000–2016 period. The EVI values close to 1 reflect intense vegetation and crop growth, whereas the EVI values near 0 refer to bare soils and degraded lands. The VCI and TCI values fluctuated from 0% to 100%. The VCI exhibited larger spatial variations than the TCI. Similar to the TCI and VCI, the VHI values ranged from 0 to 100. For the VHI values, 0 refers to the driest condition and 100 indicates a drought-free condition (Fig. 3). The closer VHI is to 0, the more severe the drought, and vice versa. We categorized the VHI values according to the thresholds presented in Table 2. Based on the VHI results, the Negueb watershed had regularly faced droughts of variant intensity and severity during the monitoring period of 2000–2016 (Fig. 3). The lowest VHI value was detected in March 2001, showing the highest drought incidence across nearly the entire study area. While the highest VHI value (100) was recorded in 2004 and 2007. The spatial pattern of CV displayed that drought-prone areas were characterized with low CV values, while mild and no drought areas had high CV values (Fig. 4). The overall CV values varied from 34.8% to 58.9%, with the lowest CV values near the upstream watershed and higher CV values in the downstream watershed. The mean VHI values ranged from 42 to 54, with most of the map showing high VHI values. The mean VHI value in the entire watershed was 48 (Fig. 4b). The drought frequency during 2000–2016 was 76.5% (Fig. 4c). Despite the high drought frequency, extreme drought events occurred rarely. For instance, only two extreme dry spells were revealed in 2001 and 2013. However, severe and moderate droughts appeared more frequently and they were detected in 2000, 2001, 2002, 2011, 2013, and 2016. Mild droughts prevailed throughout the study period excluding 2004, 2006, 2007, and 2012, which were identified as drought-free years. The drought frequency map (Fig. 4c) was produced to reveal the total number of drought events (VHI<40), over the considered period. The frequency values ranged from 24% to 36%, with the upper part of the watershed experiencing more drought events than the plains (Fig. 4c). These dry spells, expressed by low VHI values, were mostly distributed in the eastern and central regions. The topography and the low rainfall were attributed as major drivers for such low VHI values in these areas.

3.2 Soil erosion estimation

Soil erosion is a major issue in arid environments of southern Tunisia, exacerbated by long-lasting droughts. We used the GIS-based RUSLE model in this study to ensure a quantitative and consistent soil loss estimation in the Negueb watershed (Fig. 5).

3.2.1 Results of *R* factor

The values of *R* factor ranged from 56.36 to 169.03 MJ·mm/(hm^2·h·a) in the Negueb watershed (Fig. 5a). The values of *R* factor increased from east to west. It was low in the downstream of the study area, particularly in the northcentral and northeast regions (*R* factor<100.00 MJ·mm/(hm^2·h·a)). Higher values of *R* factor were concentrated mostly in higher elevations near the headwaters of the watershed (southwest) in foothills and mountainous regions.

3.2.2 Results of *LS* factor

Slope length and steepness are crucial factors controlling soil erosion mechanisms. The *LS* factor was extracted from DEM map. The elevation of the watershed varied from 110 to 690 m. The values of *LS* factor ranged from 0.03 to 13.03. The eastern section of the watershed has high and steep slopes (*LS* factor>10.00). Whereas, the eastern section has long gentler slopes (*LS* factor near 0.00). Lower values of *LS* factor covered the majority of the watershed (64%) and were focused in the central and downstream regions to the east. In the foothills between the mountains and plains, the values of *LS* factor between 2.00 and 6.00 were second most abundant observed in

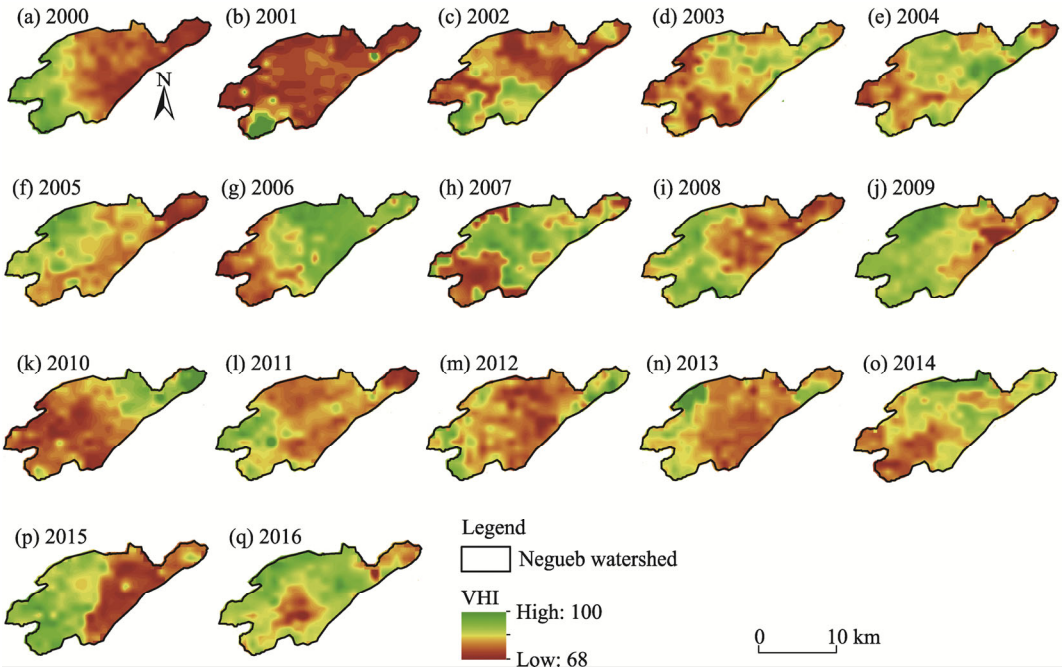

Fig. 3 Spatiotemporal drought severity in the study area during 2000–2016 (a–q)

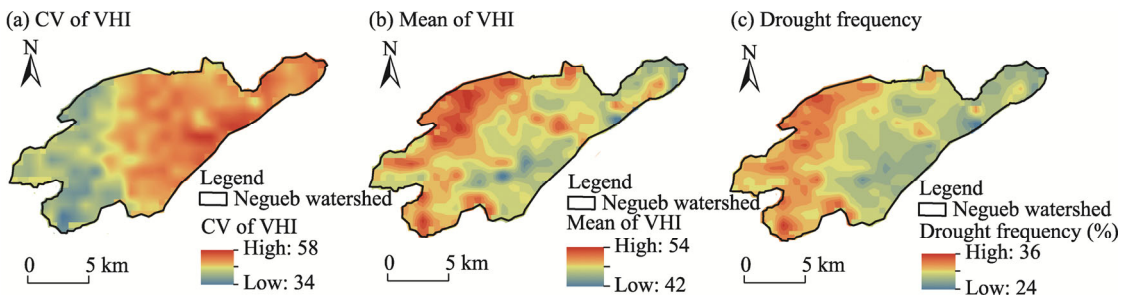

Fig. 4 Maps of coefficient of variation (CV; a) and mean (b) of VHI and drought frequency (c)

the watershed (26%). The remaining 10% of the values of *LS* factor were observed generally in areas characterized as mountainous with high elevation and steep high slopes. Thus, steepness increased from east to west. The *LS* factor was in strong agreement with soil loss and appeared to be a chief contributor of erosional loss in the watershed.

3.2.3 Results of *P* factor

The *P* factor depends not only on the agricultural practices or the anti-erosion management, but also on slope. In this study, we determined the values of *P* factor according to the slope. Low and medium values of *P* factor between 0.10 and 0.18 were assigned to areas with low and moderate slopes for areas dispersed over the plains and foothills along a south-east region (Fig. 5c). Higher values of *P* factor (0.35) were assigned in the areas with steep slopes in the upstream and northern regions. Most of the region (56%) had a low value of *P* factor (0.10) in the study area.

3.2.4 Results of *K* factor

We calculated the values of *K* factor based on soil physical and chemical properties. The values of *K* factor in the study area varied from 0.030 to 0.080 t·hm^2·h/(hm^2·MJ·mm) (Fig. 5d). Raw mineral soils, with a *K* factor of 0.030 t·hm^2·h/(hm^2·MJ·mm), were predominant in the watershed, covering 38% of the total surface. Due to water erosion, slightly evolved alluvial soils were also present (35%) and had a higher *K* factor (0.080 t·hm^2·h/(hm^2·MJ·mm)). The western headwaters region had both very low and very high values of *K* factor because of the mixed alluvial soils with raw

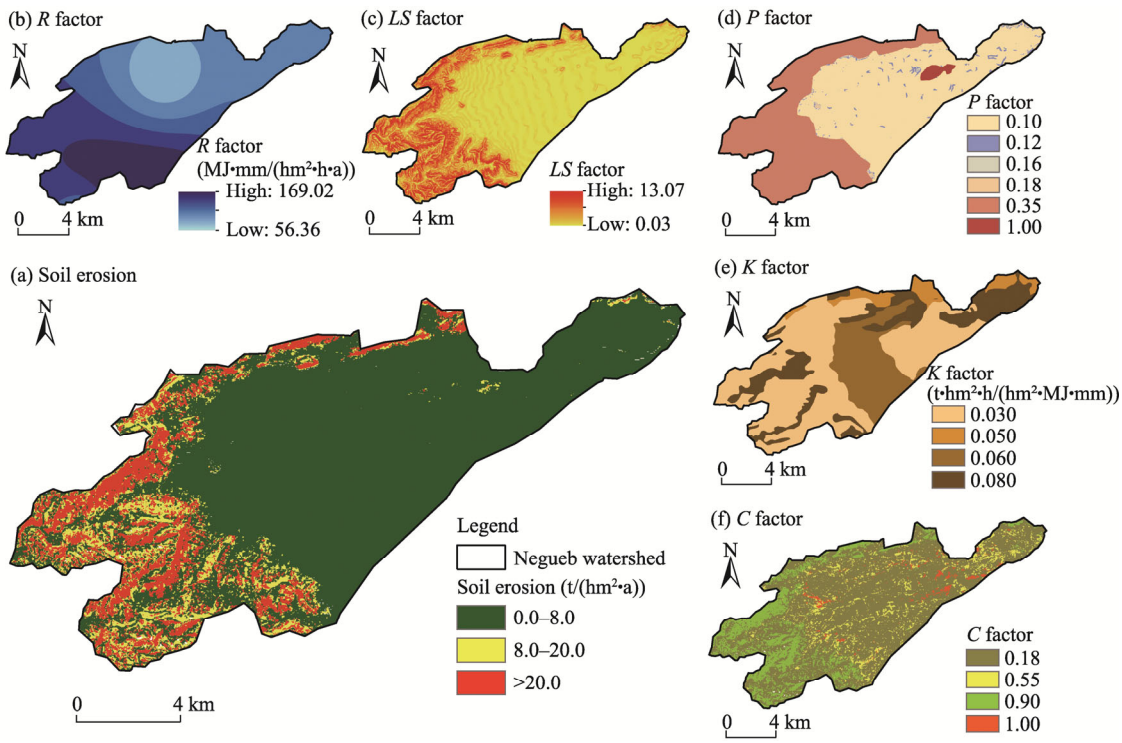

Fig. 5 Soil erosion map (a) with *R* factor (b), *LS* factor (c), *P* factor (d), *K* factor (e), *C* factor (f)

mineral soils. Areas with isohumic soils (the value of *K* factor=0.050 t•hm^2•h/(hm^2•MJ•mm)) were observed across the plains. These shallow soils with sandy to sandy-loamy texture were formed on gently sloping glacis and undergo regular hydrologic erosion, resulting in coarse elements on the surface.

3.2.5 Results of *C* factor

The values of *C* factor varied between 0.18 for croplands and 1.00 for bare soils. A *C* factor map was produced representing the different LULC types' sensitivities to erosive processes (Fig. 5e). According to the LULC map, we can find five LULC types, namely croplands behind Jessours, croplands behind Tabias, rangelands, bare soils, and bedrocks. The lowest value of *C* factor (0.18) was attributed to croplands behind Jessours and Tabias categories. The value of *C* factor was 0.55 for rangelands, 0.18 for croplands, and 1.00 for bare soils. The highest sensitivities to erosion were attributed to bare soils and bedrocks in the western watershed upstream.

3.2.6 Soil loss estimation

We estimated the potential erosion in the Negueb watershed (Fig. 5). The soil erosion map depicted erosion rates from 0.0 to 72.0 t/(hm^2•a), with a mean erosion rate of 1.8 t/(hm^2•a). For clearer spatial visualization, soil erosion was categorized into three classes. The first category included areas with low soil erosion rates (<8.0 t/(hm^2•a)). This was the major soil erosional class and constituted 86% of the total watershed area, covering most of the low elevation plains and downstream regions. The second category included areas with medium soil erosion rates between 8.0 and 20.0 t/(hm^2•a). This covered 10% of the total watershed area, occupying mainly the foothills. The last category was areas with high erosion (>20.0 t/(hm^2•a)). This group accounted for 3% of the total watershed area, and is concentrated in the upstream mountains, characterized by high elevation, rugged terrain, and friable soils. High soil erosion rates were generally associated with areas having high values of *LS* factor and *K* factor. A notable gradient of diminished erosional rate was observed from west to east and from the watershed upstream to downstream.

3.3 Investigation of the relationship between droughts and soil erosion

In this study, we accessed the relational significance between soil erosion and the VHI values using Pearson correlation. The analysis showed a positive but weak correlation between soil erosion and droughts in the Negueb watershed, where the mean *r* value was 0.3. However, the spatial distribution exhibited a strong positive relationship in some parts of the watershed (Fig. 6). The correlation coefficient (*r*) values were highly spatially variable across the watershed, from –0.59 to 0.81. The upstream portion of the watershed generally exhibited a higher correlation between soil erosion and droughts, which had severe to moderate droughts and high soil erosion rates. Generally, high-elevated areas had severe drought conditions and high soil erosion rates. While low soil erosion and moderate or even drought-free conditions were observed in the low elevation areas in the foothills and plains (Figs. 3 and 5). This high variation in elevation resulted in the reduction of correlation values.

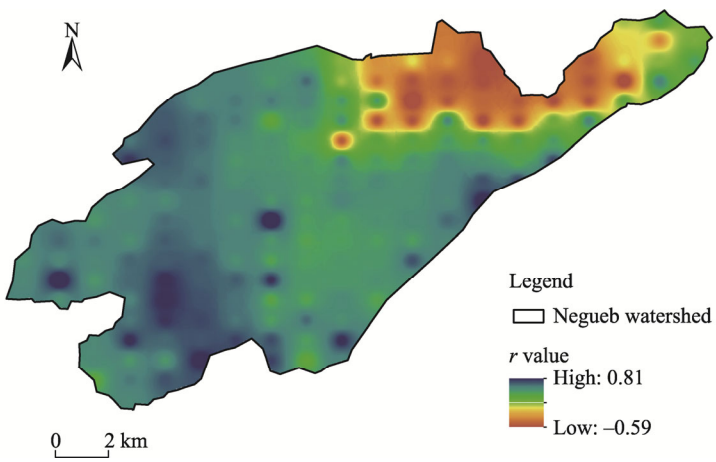

Fig. 6 Correlation coefficient (*r*) between soil loss and droughts

4 Discussion

4.1 Drought characterization in terms of severity, frequency, and duration

In arid and semi-arid regions, critical events such as droughts and soil erosion linked to climate change are problematic challenges for local populations and ecosystems, especially because these problems are trending toward increased frequency and intensity (Pachauri et al., 2014; Liu et al., 2023). Therefore, monitoring droughts and soil erosion and understanding their interconnectedness are necessary for mitigating their harmful effects. This study employed the VHI as a basic parameter to detect drought regularity, which showed that the Negueb watershed was frequently affected by droughts (Fig. 3). The spatiotemporal frequency analysis highlighted that droughts were most common in the steeper mountainous and foothills areas. These results are consistent with previous studies reporting that mountainous areas are more vulnerable to climate change, particularly droughts, than low-elevation areas (Rangwala and Miller, 2012; Pepin et al., 2015; Alamdarloo et al., 2018; Gidey et al., 2018; Mbiriri et al., 2018; Dahal et al., 2021). Feng et al. (2020) confirmed the elevation-dependent droughts in the Qinghai plateau of China. Arid mountainous regions are particularly vulnerable, as a continuous warming trend at high elevations could significantly alter hydrologic cycles in mountains, leading to a flow reduction. It is important to consider the influence of the Mediterranean Sea on the annual precipitation budget in this study area. Extreme droughts were rare, with a frequency of just 18%, consistent with previous studies in Tunisia and other Mediterranean regions (Ellouze et al., 2009; Feki et al., 2012; Bayer Altin and Altin, 2021). The Negueb watershed experienced its worst drought with respect to duration, intensity, and spatial extent during 2000–2002 period. The variable

intra-seasonal precipitation along with the low seasonal mean precipitation were the main explanations for this severe dry spell. Consequences of this drought period were observed in the local agricultural productivity, resulting in enormous economic losses as mentioned in the FAO report and other studies (Gargouri et al., 2010; FAO, 2016; Verner et al., 2018). Results were similar throughout the Mediterranean region in neighboring countries like Algeria, Morocco, Italy, and Greece (Rojas et al., 2011; Ezzine et al., 2014; Cook et al., 2016; Haied et al., 2017; Ballah and Benaabidate, 2021). Similar findings were also reported from Europe and West Africa (Bonaccorso et al., 2013; Bayissa et al., 2021). The drought severity detected with the VHI was consistent with the drought events identified using the SPI in the same region (Terwayet Bayouli et al., 2023). Thus, the VHI is conceived as a reliable indicator for drought monitoring in Tunisia. The VHI values from the growing season showed that over dry regions, vegetation was more prone to droughts when it is at its peak activity, consistent with previous findings of Bento et al. (2020). Additionally, it is observed that sandy-textured areas challenged more severe drought condition than areas with silty-clay texture having higher water storage capacity. This indicates soil texture also contributes to the drought spatial distribution in the Negueb watershed.

4.2 Quantification of the average annual soil loss

The RUSLE model has been identified as an efficient tool to determine soil loss that is effective in rurally-settled watersheds with fragile soil resources and irregular precipitation, such as the Negueb watershed (Napoli et al., 2016; Phinzi and Ngetar, 2019). The results showed the *R* factor increased from east to west, along an elevation gradient, which appeared to play an influencing role on the variable erosivity. The *K* factor showed four main categories, predominantly soils with moderate to high permeability. Since erodibility increases in sandy soils whereas clay textured soils are capable to resist erosion processes, soil texture and carbon content are indicators of soil erosion intensity (Duiker et al., 2001). The *K* factor also depends on dry weather conditions; therefore, drought effects should be considered for more accurate *K* factor assessment (Baskan, 2021). The spatial distribution of *LS* factor was mainly proportional to the overall topography due to the high waterflow velocity. Therefore, the *LS* factor was an inducing factor of soil erosion in the Negueb watershed. The effect of LULC on soil erosion is elucidated in the *C* factor analysis (He et al., 2020). Dense vegetation areas in the plains had lower values of *C* factor, whereas bare lands and mountainous areas had higher values of *C* factor. This indicated a greater susceptibility to soil erosion in the later compared to the former and validated the remotely sensed data performance to estimate the *C* factor (Guo et al., 2023). Soil and water conservation techniques, such as retention ditches and bench terraces, were implemented in the Negueb watershed as part of a national erosion control strategy. Although the upstream and northern parts had the highest values of *P* factor, soil erosion vulnerability was greater in these regions. This may be explained by the conservation techniques efficiency decreasing with increased slope. Therefore, implementation of more appropriate soil management techniques and maintenance of Jessours at the upstream areas, where soil erosion was intensified, are encouraged to mitigate soil loss. The soil erosion intensified from east to west in the Negueb watershed, where the low-lying plains region was generally at low soil erosive risk. The annual soil erosion ranged from 0.0 to 72.0 t/(hm^2·a), with an average of 1.8 t/(hm^2·a). These results were in accordance with previous findings obtained by other studies in Tunisia conducted under arid climate (Chafai et al., 2020). The drought susceptibility, along with dry soil characteristics, could explain the high soil erosion risk in the upstream watershed. These regions characterized by high landforms and steep slopes were covered mostly by sparse rangelands and arboriculture. Additionally, they were occupied by raw mineral soils and slightly developed alluvial soils having a strong erodibility. While all RUSLE model parameters impact the soil erosion rate, each factors had different impact degree on the soil erosion rate. The greatest contributor to soil erosion in the Negueb watershed was the *LS* factor, in accordance with other findings reporting that erosion increases exponentially with the slope inclination degree (Elbouqdaoui et al., 2005; Markose and Jayappa, 2016). The *K* factor and *R* factor were also identified as determinant factors that augment soil erosion in the region.

The *C* factor and *P* factor had less impact in triggering soil erosion. Our findings are in agreement with a previous regional study of modeled soil erosion using the RUSLE model in El-Hamma catchment of Tunisia, a region geographically near this study area and with similar climatic and environmental characteristics, that showed mountainous regions in a catchment were under greater soil erosion risk (Jemai et al., 2021). Similar results were reached by researchers in neighboring Algeria and Morocco (Toubal et al., 2018; Amellah and el Morabiti, 2021; Bensekhria and Bouhata, 2022). At the global scale, Zhao et al. (2021) showed that extremely severe soil erosion was mostly concentrated in the mountainous areas.

To support the soil erosion results, we conducted a spatial scale validation through photointerpretation in TerraIncognita and Google Earth software, followed by terrain observations. The validation process highlighted that the areas most affected by water erosion were mainly located upstream along the mountains that define the watershed western boundary (Figs. 7 and 8). In this region, the landforms were visible due to the shallow soil surface and the limited vegetation. The bare hillsides pronounced intense water erosion signs exposing patinated and cantilevered limestones that detached in large sections to form scree talus at the foothill. The erosive action of flowing water scoured deep valleys into the fine rocks and deposited material down gradient as foothills. The erosional deposits of coarse to fine sediments accumulated downstream and built-up alluvial cones or loess layers.

The areas most affected by droughts visually coincided with areas having the highest soil erosion rates; which were located upstream (Figs. 4c and 5). Soil erosion in these mountainous regions may be primarily attributed to the dry soil characteristics, drought susceptibility, sparse vegetation cover, and poor management practices.

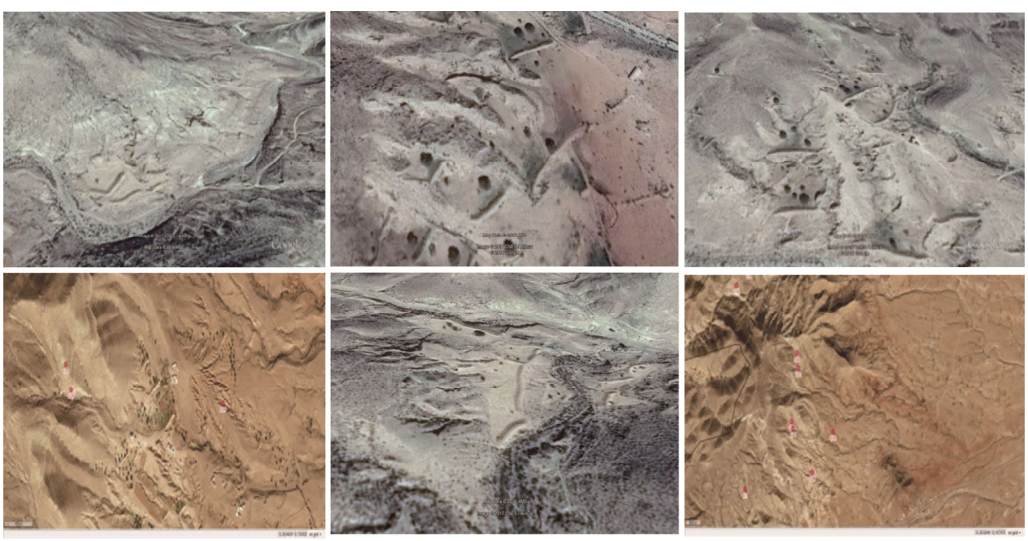

Fig. 7 Identification of areas affected by severe water erosion through Google Earth and TerraIncognita software

4.3 Interrelation between droughts and soil erosion

The correlation between the average soil erosion rate and droughts over the Negueb watershed revealed the significance of interrelatedness. Correlation analysis showed a positive relationship (r=0.3) between soil erosion and droughts. Although this broad correlation was not strong, a spatial distribution analysis of the connection between droughts and soil erosion showed a strong correlation in the upstream, which was also the most vulnerable to both. Yu et al. (2021) reported that the relationship between drought frequency and soil erosion intensity had a correlation relationship (r=0.27), showing a similar consistent. Soil erosion in the Negueb watershed intensified drought effects, which was detrimental to local and regional ecosystem services. Under intense erosional weathering, decreased soil depth results in a decreased soil moisture

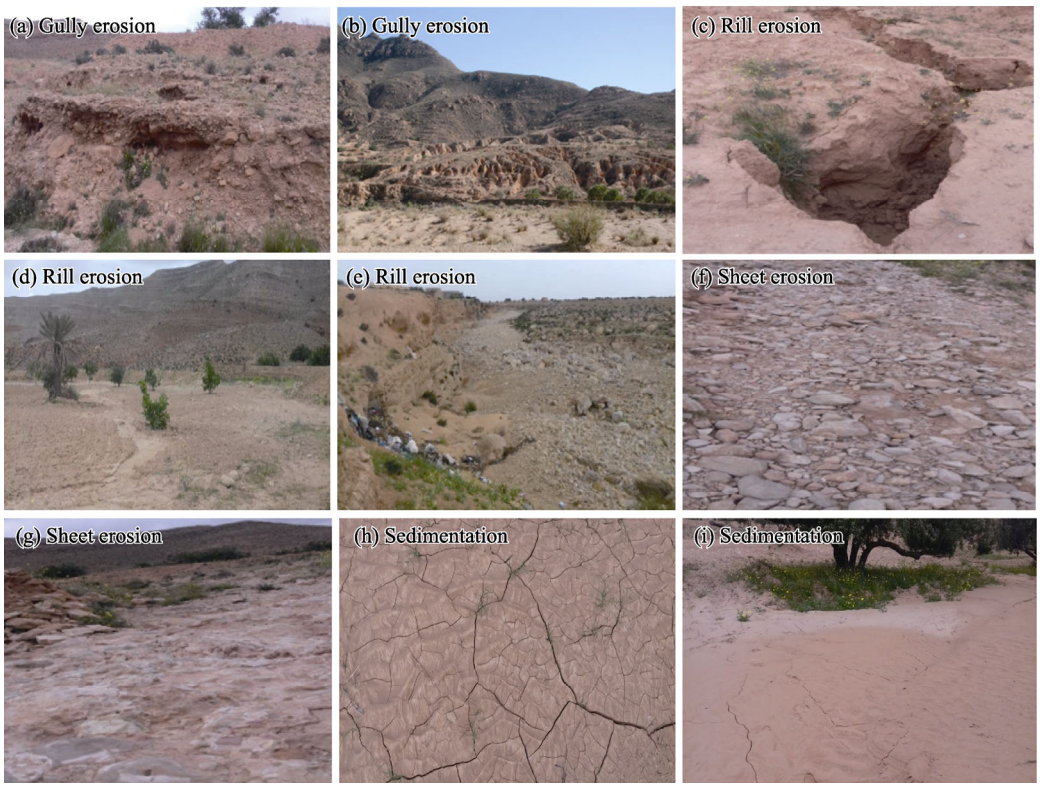

Fig. 8 Visited sites affected by different water erosion types in the Negueb watershed. (a and b), gully erosion; (c, d, and e), rill erosion; (f and g), sheet erosion; and (h and i), sedimentation.

storage capacity (Magesh and Chandrasekar, 2016). A reduction in soil moisture for prolonged periods accordingly impedes vegetation growth and leads to a decay of natural vegetation and crops (Zhu et al., 2022). As a consequence of this climate feedback, an area can become increasingly vulnerable to droughts. Similarly, droughts can trigger soil erosional processes as dry soils are more vulnerable to mass movement by wind or water. As soils dry and the vegetative cover is diminished, there is a subsequent reduction in water infiltration and an increase in surface runoff (Le Houérou, 1996; Hewelke et al., 2022). Each of which contributes to developing soils highly vulnerable to accelerated erosion (Ahn et al., 2013; Bombino et al., 2019). Intense rainfall events, such as the torrential precipitation in the Negueb watershed, following dry periods promote soil particle detachment and transport resulting in the loss of fertile topsoil. This poses a significant ecological and economical threat to land productivity, particularly in arid environments. While ground-truthing RUSLE model factors on field observations, it was observed that uncontrolled runoff from terraces in mountainous regions resulted in gully formation (Fig. 8). Rill and sheet erosion were more common as a result of LULC changes, inappropriate soil management, agricultural and anthropogenic activities, and livestock overgrazing. Therefore, the integration of effective land management practices ranks as the highest priority for future interventions to mitigate soil erosion. Improving soil resilience by increasing carbon and phosphorus inputs through compost, organic manures, and soil conservation measures on sloping lands is proposed as a "triple win" solution to reverse degradation, build resilience to climate change, and promote sustainability in fragile arid environments.

5 Conclusions

This study assessed factors controlling drought conditions and soil erosion processes in the Negueb watershed, an arid region in southeastern Tunisia. Drought conditions were analyzed

using the VHI, generated by combining the VCI and TCI indices, from 2000 to 2016. The RUSLE model was incorporated to estimate soil erosion and the interrelation between droughts and soil erosion was investigated using Pearson correlation. Results revealed that droughts were a recurrent phenomenon during 2000–2016. Further, the spatial distribution of droughts in the watershed showed greater vulnerability in the upstream in the western higher elevations. The overall average soil erosion rate was 1.8 t/(hm^2·a). Slope length and steepness factor was the most influencing factor triggering soil erosion. Analysis of the relationship between droughts and soil erosion showed a positive weak correlation (r=0.3), while the spatial correlation coefficient between soil erosion and droughts ranged from –0.5 to 0.8, with strong and significant correlations in regions of frequent droughts and high soil erosion rates. Therefore, soil erosion was found to be related to droughts. The RUSLE model and the VHI proved to be efficient tools for assessing soil erosion and droughts and identified the upstream areas being very susceptible to climatic variations and a hotspot for soil conservation management. However, some limitations were associated with accurate erosion risk modeling using the RUSLE model, such as input data resolution and validation given the local data scarcity. Therefore, it is recommended to focus resources on high-resolution imagery particularly for the vegetation as it is a significant factor for soil erosion and droughts. Future directions for this study should include extension to erosion and drought impacts on land productivity in the Negueb watershed.

Conflict of interest

The authors declare that they have no known competing financial interests or personal relationships that could have appeared to influence the work reported in this paper.

Acknowledgements

We would like to thank Dr. Robert A. ROOT for his contribution to revising and editing the manuscript. The first author would like to thank Chinese Academy of Sciences (CAS) and The World Academy of Science (TWAS) for providing financial support.

Author contributions

Conceptualization: Olfa TERWAYET BAYOULI; Data curation: Olfa TERWAYET BAYOULI, Houssem TERWAYET BAYOULI; Methodology: Olfa TERWAYET BAYOULI; Investigation and Formal analysis: Olfa TERWAYET BAYOULI, ZHANG Wanchang; Writing - original draft preparation: Olfa TERWAYET BAYOULI; Writing - review and editing: ZHANG Wanchang, Olfa TERWAYET BAYOULI, Houssem TERWAYET BAYOULI; Supervision: ZHANG Wanchang; Software: Olfa TERWAYET BAYOULI, Houssem TERWAYET BAYOULI; Validation and Visualization: Olfa TERWAYET BAYOULI, ZHANG Wanchang.

References

Abdelhak M. 2022. Soil improvement in arid and semiarid regions for sustainable development. Natural Resources Conservation and Advances for Sustainability, doi: 10.1016/B978-0-12-822976-7.00026-0.

Ahn S, Doerr S H, Douglas P, et al. 2013. Effects of hydrophobicity on splash erosion of model soil particles by a single water drop impact. Earth Surface Processes and Landforms, 38(11): 1225–1233.

Alamdarloo E H, Manesh M B, Khosravi H. 2018. Probability assessment of vegetation vulnerability to drought based on

remote sensing data. Environmental Monitoring and Assessment, 190: 702, doi: 10.1007/s10661-018-7089-1.

Amellah O, el Morabiti K. 2021. Assessment of soil erosion risk severity using GIS, remote sensing and RUSLE model in Oued Laou Basin (north Morocco). Soil Science Annual, 72(3): 142530, doi: 10.37501/soilsa/142530.

Arnoldus H M J. 1977. Predicting Soil Losses Due to Sheet and Rill Erosion. FAO Conservation Guide 1: Guidelines for Watershed Management. Rome: FAO.

Ballah A, Benaabidate L. 2021. Assessing the performance of various meteorological drought indices in capturing historic droughts in the south of Algeria. Arabian Journal of Geosciences, 14(13): 1289, doi: 10.1007/s12517-021-07556-8.

Baskan O. 2021. Analysis of spatial and temporal changes of RUSLE-K soil erodibility factor in semi-arid areas in two different periods by conditional simulation. Archives of Agronomy and Soil Science, doi: 10.1080/03650340.2021.1922673.

Bayer Altin T, Altin B N. 2021. Response of hydrological drought to meteorological drought in the eastern Mediterranean Basin of Turkey. Journal of Arid Land, 13(5): 470–486.

Bayissa Y, Moges S, Melesse A, et al. 2021. Multi-dimensional drought assessment in Abbay/Upper Blue Nile Basin: The importance of shared management and regional coordination efforts for mitigation. Remote Sensing, 13(9): 1835, doi: 10.3390/rs13091835.

Belaid H, Habaieb H. 2015. Soil aggregate stability in a Tunisian semi-arid environment with reference to fractal analysis. Journal of Soil Science and Environmental Management, 6(2): 16–23.

Ben Rhouma A, Hermassi T, Habaieb H. 2018. Water erosion modeling in a Mediterranean semi-arid catchment using USLE/GIS (El Gouazine, Central Tunisia). Journal of New Sciences, 50: 3071–3081.

Bensekhria A, Bouhata R. 2022. Assessment and mapping soil water erosion using RUSLE approach and GIS tools: case of oued el-Hai watershed, Aurès West, Northeastern of Algeria. ISPRS International Journal of Geo-Information, 11(2): 84, doi: 10.3390/ijgi11020084.

Bento V A, Gouveia C M, DaCamara C C, et al. 2020. The roles of NDVI and land surface temperature when using the vegetation health index over dry regions. Global and Planetary Change, 190: 103198, doi: 10.1016/j.gloplacha.2020.103198.

Bombino G, Denisi P, Gómez J A, et al. 2019. Water infiltration and surface runoff in steep clayey soils of olive groves under different management practices. Water, 11(2): 240, doi: 10.3390/w11020240.

Bonaccorso B, Peres D J, Cancelliere A, et al. 2013. Large scale probabilistic drought characterization over Europe. Water Resources Management, 27(6): 1675–1692.

Borrelli P, Robinson D A, Fleischer L R, et al. 2017. An assessment of the global impact of 21st century land use change on soil erosion. Nature Communications, 8, doi: 10.1038/s41467-017-02142-7.

Brychta J, Podhrázská J, Šťastná M. 2022. Review of methods of spatio-temporal evaluation of rainfall erosivity and their correct application. CATENA, 217: 106454, doi: 10.1016/j.catena.2022.106454.

Chafai A, Brahim N, Shimi N S. 2020. Mapping of water erosion by GIS/RUSLE approach: watershed Ayda river—Tunisia study. Arabian Journal of Geosciences, 13(16): 1–14.

Cook B I, Anchukaitis K J, Touchan R, et al. 2016. Spatiotemporal drought variability in the Mediterranean over the last 900 years. Journal of Geophysical Research: Atmospheres, 121(5): 2060–2074.

Cormary Y, Masson J. 1964. Study of water and soil conservation at the Rural Engineering Research Center of Tunisia: Application of Wischmeier's soil loss formula to a typical project. ORSTOM Notebooks - Pedology Series, 2(3): 3–26. (in French)

Dahal N M, Xiong D, Neupane N, et al. 2021. Spatiotemporal analysis of drought variability based on the standardized precipitation evapotranspiration index in the Koshi River Basin, Nepal. Journal of Arid Land, 13(5): 433–454.

da Silva E C, de Albuquerque M B, de Azevedo Neto A D, et al. 2013. Drought and its consequences to plants—From individual to ecosystem. Responses of Organisms to Water Stress, 18–47.

Diodato N, Bellocchi G. 2010. MedREM, a rainfall erosivity model for the Mediterranean region. Journal of Hydrology, 387(1–2): 119–127.

Du H, Dou S, Deng X, et al. 2016. Assessment of wind and water erosion risk in the watershed of the Ningxia-Inner Mongolia Reach of the Yellow River, China. Ecological Indicators, 67: 117–131.

Duiker S, Flanagan D, Lal R. 2001. Erodibility and infiltration characteristics of five major soils of southwest Spain. CATENA, 45(2): 103–121.

DVWK. 1990. Sediment Transport in Open Channels. Berlin: German Association for Water and Land Improvement.

Eekhout J P C, de Vente J. 2022. Global impact of climate change on soil erosion and potential for adaptation through soil conservation. Earth-Science Reviews, 226: 103921, doi: 10.1016/j.earscirev.2022.103921.

Elbouqdaoui K, Ezzine H, Badraoui M, et al. 2005. Evaluation by remote sensing and SIG of potential erosion risk in the Oued Srou Basin (Middle Atlas, Morocco). International Journal of Tropical Geology, Geography and Ecology, 29: 25–36.

Ellouze M, Azri C, Abida H. 2009. Spatial variability of monthly and annual rainfall data over Southern Tunisia. Atmospheric Research, 93(4): 832–839.

Ezzine H, Bouziane A, Ouazar D. 2014. Seasonal comparisons of meteorological and agricultural drought indices in Morocco using open short time-series data. International Journal of Applied Earth Observation and Geoinformation, 26: 36–48.

Fang G, Yuan T, Zhang Y, et al. 2019. Integrated study on soil erosion using RUSLE and GIS in Yangtze River Basin of Jiangsu Province (China). Arabian Journal of Geosciences, 12(5): 1–13.

FAO. 1977. Conservation Guide 1. Guidelines for Watershed Management. Rome: FAO, 147–179.

FAO. 2015. World Reference Base for Soil Resources 2014. International Soil Classification System for Naming Soils and Creating Legends for Soil Maps. [2022-11-23]. https://www.fao.org/3/i3794en/I3794en.pdf.

FAO. 2016. Food Outlook - Biannual Report on Global Food Markets. Rome: FAO, 100.

Feki H, Slimani M, Cudennec C. 2012. Incorporating elevation in rainfall interpolation in Tunisia using geostatistical methods. Hydrological Sciences Journal, 57(7): 1294–1314.

Feng W, Lu H, Yao T, et al. 2020. Drought characteristics and its elevation dependence in the Qinghai-Tibet plateau during the last half-century. Scientific Reports, 10(1): 1–11.

Ferro V, Giordano G, Iovino M. 1991. Isoerosivity and erosion risk map for Sicily. Hydrological Sciences Journal, 36(6): 549─564.

Floret C, Pontanier R. 1982. Aridity in Pre-Saharan Tunisia: Climate, Soil, Vegetation and Development. Paris: ORSTOM. (in French)

Gamoun M. 2016. Rain use efficiency, primary production and rainfall relationships in desert rangelands of Tunisia. Land Degradation & Development, 27(3): 738–747.

Gargouri K, Laajimi A, Chebil A, et al. 2010. Drought occurrence and its impact on olive production and cereals in Tunisia. Séminaires Méditerranéens, (95): 41–47.

Genin D, Guillaume H, Ouessar M, et al. 2006. Between Desertification and Development: the Tunisian Jeffara. Tunis: IRD. (in French)

Ghoneim E, Dorofeeva A, Benedetti M, et al. 2017. Vegetation drought analysis in Tunisia: a geospatial investigation. Journal of Atmospheric & Earth Sciences, 1(2), doi: 10.24966/AES-8780/100002.

Gidey E, Dikinya O, Sebego R, et al. 2018. Analysis of the long-term agricultural drought onset, cessation, duration, frequency, severity and spatial extent using Vegetation Health Index (VHI) in Raya and its environs, Northern Ethiopia. Environmental Systems Research, 7(1): 13, doi: 10.1186/s40068-018-0115-z.

Guo B, Lu M, Fan Y, et al. 2023. A novel remote sensing monitoring index of salinization based on three-dimensional feature space model and its application in the Yellow River Delta of China. Geomatics, Natural Hazards and Risk, 14(1): 95–116.

Haied N, Foufou A, Chaab S, et al. 2017. Drought assessment and monitoring using meteorological indices in a semi-arid region. Energy Procedia, 119: 518–529.

Hazaymeh K, Hassan Q K. 2017. A remote sensing-based agricultural drought indicator and its implementation over a semi-arid region, Jordan. Journal of Arid Land, 9(3): 319–330.

He Q, Dai X A, Chen S. 2020. Assessing the effects of vegetation and precipitation on soil erosion in the Three-River Headwaters Region of the Qinghai-Tibet Plateau, China. Journal of Arid Land, 12(5): 865–886.

Heim R R. 2002. A review of twentieth-century drought indices used in the United States. Bulletin of the American Meteorological Society, 83(8): 1149–1166.

Hewelke E, Gozdowski D, Korc M, et al. 2022. Influence of soil moisture on hydrophobicity and water sorptivity of sandy soil no longer under agricultural use. CATENA, 208: 105780, doi: 10.1016/j.catena.2021.105780.

Imamoglu A, Dengiz O. 2017. Determination of soil erosion risk using RUSLE model and soil organic carbon loss in Alaca catchment (Central Black Sea region, Turkey). Rendiconti Lincei, 28: 11–23.

Jemai S, Kallel A, Agoubi B, et al. 2021. Soil erosion estimation in arid area by USLE model applying GIS and RS: Case of Oued El Hamma catchment, south-eastern Tunisia. Journal of the Indian Society of Remote Sensing, 49(6): 1293–1305.

Karnieli A, Bayasgalan M, Bayarjargal Y, et al. 2006. Comments on the use of the vegetation health index over Mongolia. International Journal of Remote Sensing, 27(10): 2017–2024.

Kefi M, Yoshino K, Setiawan Y. 2012. Assessment and mapping of soil erosion risk by water in Tunisia using time series MODIS data. Paddy and Water Environment, 10(1): 59–73.

Keyantash J, Dracup J A. 2002. The quantification of drought: An evaluation of drought indices. Bulletin of the American Meteorological Society, 83(8): 1167–1180.

Kogan F N. 1995. Application of vegetation index and brightness temperature for drought detection. Advances in Space Research, 15(11): 91–100.

Kogan F, Guo W, Strashnaia A, et al. 2016. Modelling and prediction of crop losses from NOAA polar-orbiting operational satellites. Geomatics, Natural Hazards and Risk, 7(3): 886–900.

König H J, Sghaier M, Schuler J, et al. 2012. Participatory impact assessment of soil and water conservation scenarios in Oum Zessar watershed, Tunisia. Environmental Management, 50(1): 153–165.

Lazzari M, Gioia D, Piccarreta M, et al. 2015. Sediment yield and erosion rate estimation in the mountain catchments of the Camastra artificial reservoir (Southern Italy): A comparison between different empirical methods. CATENA, 127: 323–339.

Le Houérou H N. 1996. Climate change, drought and desertification. Journal of Arid Environments, 34(2): 133–185.

Liu B Y, Nearing M A, Shi P J, et al. 2000. Slope length effects on soil loss for steep slopes. Soil Science Society of America Journal, 64(5): 1759–1763.

Liu W, Kogan F. 1996. Monitoring regional drought using the vegetation condition index. International Journal of Remote Sensing, 17(14): 2761–2782.

Liu Y, Guo B, Lu M, et al. 2023. Quantitative distinction of the relative actions of climate change and human activities on vegetation evolution in the Yellow River Basin of China during 1981–2019. Journal of Arid Land, 15(1): 91–108.

Lloyd-Hughes B. 2013. The impracticality of a universal drought definition. Theoretical and Applied Climatology, 117, doi: 10.1007/s00704-013-1025-7.

Lu S, Liu B, Hu Y, et al. 2020. Soil erosion topographic factor (LS): Accuracy calculated from different data sources. CATENA, 187: 104334, doi: 10.1016/j.catena.2019.104334.

Lucatello S, Huber-Sannwald E. 2020. Sustainable Development Goals and Drylands: Addressing the Interconnection. [2022-11-20]. https://link.springer.com/chapter/10.1007/978-3-030-22464-6_2.

Magesh N, Chandrasekar N. 2016. Assessment of soil erosion and sediment yield in the Tamiraparani sub-basin, South India, using an automated RUSLE-SY model. Environmental Earth Sciences, 75(16): 1–17.

Markose V J, Jayappa K. 2016. Soil loss estimation and prioritization of sub-watersheds of Kali River basin, Karnataka, India, using RUSLE and GIS. Environmental Monitoring Assessment, 188(4): 1–16.

Marumbwa F M, Cho M A, Chirwa P W. 2020. An assessment of remote sensing-based drought index over different land cover types in southern Africa. International Journal of Remote Sensing, 41(19): 7368–7382.

Masroor M, Sajjad H, Rehman S, et al. 2022. Analysing the relationship between drought and soil erosion using vegetation health index and RUSLE models in Godavari middle sub-basin, India. Geoscience Frontiers, 13(2): 101312, doi: 10.1016/j.gsf.2021.101312.

Mbiriri M, Mukwada G, Manatsa D. 2018. Influence of altitude on the spatiotemporal variations of meteorological droughts in mountain regions of the free state province, South Africa (1960–2013). Advances in Meteorology, 2018: 5206151, doi: 10.1155/2018/5206151.

MEHAT. 2012. Atlas of Medenine Governorate. Tunis: Ministry of Housing Equipment and Territorial Planning of Tunisia, 104. (in French)

Middleton N, Kang U. 2017. Sand and dust storms: Impact mitigation. Sustainability, 9(6): 1053, doi: 10.3390/su9061053.

Mtimet A. 2001. Soils of Tunisia. Options Méditerranéennes, 34: 243–268.

Napoli M, Cecchi S, Orlandini S, et al. 2016. Simulation of field-measured soil loss in Mediterranean hilly areas (Chianti, Italy) with RUSLE. CATENA, 145: 246–256.

Omuto C, Vargas R. 2009. Combining pedometrics, remote sensing and field observations for assessing soil loss in challenging drylands: a case study of northwestern Somalia. Land Degradation & Development, 20(1): 101–115.

Pachauri R K, Allen M R, Barros V R, et al. 2014. Climate Change 2014: Synthesis Report. Contribution of Working Groups I, II and III to the Fifth Assessment Report of the Intergovernmental Panel on Climate Change, IPCC. [2022-11-22].

https://www.ipcc.ch/site/assets/uploads/2018/05/SYR_AR5_FINAL_full_wcover.pdf.

Parviz L. 2016. Determination of effective indices in the drought monitoring through analysis of satellite images. Agriculture and Forestry, 62(1): 305, doi: 10.17707/AgricultForest.62.1.34.

Patil R J. 2018. Spatial techniques for soil erosion estimation. In: Patil R J. Spatial Techniques for Soil Erosion Estimation: Remote Sensing and GIS Approach. Switzerland: Springer.

Pei F, Wu C, Liu X, et al. 2018. Monitoring the vegetation activity in China using vegetation health indices. Agricultural and Forest Meteorology, 248: 215–227.

Pepin N, Bradley R S, Diaz H F, et al. 2015. Elevation-dependent warming in mountain regions of the world. Nature Climate Change, 5(5): 424–430.

Pepin Y, Hammouda N. 2012. Variability of rainfall intensity in the Tangier region over a period of 30 years (1980–2010). Revue marocaine des sciences agronomiques et vétérinaires, 1(1): 23–27. (in French)

Peri P L, Lasagno R G, Chartier M, et al. 2021. Soil erosion rates and nutrient loss in rangelands of southern Patagonia. In: The Encyclopedia of Conservation—Reference Module in Earth Systems and Environmental Sciences. Netherlands: Elsevier.

Phinzi K, Ngetar N S. 2019. The assessment of water-borne erosion at catchment level using GIS-based RUSLE and remote sensing: A review. International Soil and Water Conservation Research, 7(1): 27–46.

Prasannakumar V, Vijith H, Abinod S, et al. 2012. Estimation of soil erosion risk within a small mountainous sub-watershed in Kerala, India, using Revised Universal Soil Loss Equation (RUSLE) and geo-information technology. Geoscience Frontiers, 3(2): 209–215.

Qiu J, Shen Z, Leng G, et al. 2021. Synergistic effect of drought and rainfall events of different patterns on watershed systems. Scientific Reports, 11(1): 1–18.

Rahmati O, Tahmasebipour N, Haghizadeh A, et al. 2017. Evaluating the influence of geo-environmental factors on gully erosion in a semi-arid region of Iran: An integrated framework. Science of the Total Environment, 579: 913–927.

Rangwala I, Miller J R. 2012. Climate change in mountains: a review of elevation-dependent warming and its possible causes. Climatic Change, 114(3): 527–547.

Reichhuber A, Gerber N, Mirzabaev A, et al. 2019. The land-drought nexus enhancing the role of land-based interventions in drought mitigation and risk management. [2022-11-22]. https://www.unccd.int/resources/reports/land-drought-nexus-enhancing-role-land-based-interventions-drought-mitigation-and.

Renard K G, Freimund J R. 1994. Using monthly precipitation data to estimate the R-factor in the revised USLE. Journal of Hydrology, 157(1–4): 287–306.

Renard K G, Foster G R, Weesies G A, et al. 1997. Predicting Soil Erosion by Water - A Guide to Conservation Planning with the Revised Universal Soil Loss Equation (RUSLE). Washington DC: United States Government Printing.

Renard K G, Laflen J, Foster G, et al. 2017. The revised universal soil loss equation. Soil Erosion Research Methods, 105–126.

Rhee J, Jm J, Carbone G J. 2010. Monitoring agricultural drought for arid and humid regions using multi-sensor remote sensing data. Remote Sensing of Environment, 114(12): 2875–2887.

Rojas O, Vrieling A, Rembold F. 2011. Assessing drought probability for agricultural areas in Africa with coarse resolution remote sensing imagery. Remote Sensing of Environment, 115(2): 343–352.

Roose E. 1977. Use of the universal soil loss equation to predict erosion in West Africa. Soil Erosion: Prediction and Control (21): 60–74.

Santra A, Mitra S S. 2020. Space-time drought dynamics and soil erosion in Puruliya district of West Bengal, India: A conceptual design. Journal of the Indian Society of Remote Sensing, 48: 1191–1205.

Schiettecatte W, Ouessar M, Gabriels D, et al. 2005. Impact of water harvesting techniques on soil and water conservation: A case study on a micro catchment in southeastern Tunisia. Journal of Arid Environments, 61(2): 297–313.

Seiler R, Kogan F, Sullivan J. 1998. AVHRR-based vegetation and temperature condition indices for drought detection in Argentina. Advances in Space Research, 21(3): 481–484.

Sghaier M, Arbi A M, Tonneau J-P, et al. 2012. Land Degradation in the Arid Jeffara Region, Tunisia. Land Use Policies for Sustainable Development: Exploring Integrated Assessment Approaches. Cheltenham: Edward Elgar Publishing.

Shen R, Huang A, Li B, et al. 2019. Construction of a drought monitoring model using deep learning based on multi-source remote sensing data. International Journal of Applied Earth Observation and Geoinformation, 79: 48–57.

Singh R P, Roy S, Kogan F. 2003. Vegetation and temperature condition indices from NOAA AVHRR data for drought

monitoring over India. International Journal of Remote Sensing, 24(22): 4393–4402.

Taamallah H. 2003. Soil Map of Jeffara. Tunis: IRA/IRD. (in French)

Tamene L, Le Q B. 2015. Estimating soil erosion in sub-Saharan Africa based on landscape similarity mapping and using the revised universal soil loss equation (RUSLE). Nutrient Cycling in Agroecosystems, 102(1): 17–31.

Terwayet Bayouli O, Zhang W, Terwayet Bayouli H. 2023. Assessment of drought characteristics and its impacts on net primary productivity (NPP) in southeastern Tunisia. Arabian Journal of Geosciences, 16(1): 26, doi: 10.1007/s12517-022-11091-5.

Toubal A K, Achite M, Ouillon S, et al. 2018. Soil erodibility mapping using the RUSLE model to prioritize erosion control in the Wadi Sahouat basin, North-West of Algeria. Environmental Monitoring Assessment, 190(4): 1–22.

Trnka M, Semeradova D, Novotný I, et al. 2016. Assessing the combined hazards of drought, soil erosion and local flooding on agricultural land: A Czech case study. Climate Research, 70, doi: 10.3354/cr01421.

Verner D, Treguer D, Redwood J, et al. 2018. Climate Variability, Drought, and Drought Management in Tunisia's Agricultural Sector. [2022-11-21]. https://documents1.worldbank.org/curated/en/318211538415630621/pdf/130406-WP-P159856-Tunisia-WEB2.pdf.

Wischmeier W H, Smith D D. 1978. Predicting Rainfall Erosion Losses: A Guide to Conservation Planning. Washington DC: Department of Agriculture, Science and Education Administration.

Wu G, Chen J, Shi X, et al. 2022. Impacts of global climate warming on meteorological and hydrological droughts and their propagations. Earth's Future, 10(3), doi: e2021EF002542.

Yang D, Kanae S, Oki T, et al. 2003. Global potential soil erosion with reference to land use and climate changes. Hydrological Processes, 17(14): 2913–2928.

Yu Y, Shen Y, Wang J, et al. 2021. Simulation and mapping of drought and soil erosion in Central Yunnan Province, China. Advances in Space Research, 68(11): 4556–4572.

Zargar A, Sadiq R, Naser B. 2011. A review of drought indices. Environmental Reviews, 19: 333–349.

Zhao Y, Liu L, Kang S, et al. 2021. Quantitative analysis of factors influencing spatial distribution of soil erosion based on geo-detector model under diverse geomorphological types. Land, 10(6): 604, doi: 10.3390/land10060604.

Zhu P, Jia X, Zhao C, et al. 2022. Long-term soil moisture evolution and its driving factors across China's agroecosystems. Agricultural Water Management, 269: 107735, doi: 10.1016/j.agwat.2022.107735.